ARTICLE

Ultraviolet Photodissociation Dynamics of DNCO+$h\nu$→D+NCO: Two Competitive Pathways

Shu Su[a,b†], Zhen Chen[a,b†], Zhi-chao Chen[a], Guo-rong Wu[a], Dong-xu Dai[a], Kai-jun Yuan[a*], Xue-ming Yang[a]

a. State Key Laboratory of Molecular Reaction Dynamics, Dalian Institute of Chemical Physics, Dalian 116023, China
b. University of Chinese Academy of Sciences, Beijing 100049, China

(Dated: Received on April 13, 2019; Accepted on May 8, 2019)

Photodissociation dynamics of DNCO+$h\nu$→D+NCO at photolysis wavelengths between 200 and 235 nm have been studied using the D-atom Rydberg tagging time-of-flight technique. Product translational energy distributions and angular distributions have been determined. Nearly statistical distribution of the product translational energy with nearly isotropic angular distribution was observed at 210−235 nm, which may come from the predissociation pathway of internal conversion from S_1 to S_0 state followed by decomposition on S_0 surface. At shorter photolysis wavelengths, in addition to the statistical distribution, another feature with anisotropic angular distribution appears at high translational energy region, which can be attributed to direct dissociation on S_1 surface. Compared with HNCO, the direct dissociation pathway for DNCO photodissociation opens at higher excitation energy. According to our assignment of the NCO internal energy distribution, dominantly bending and a little stretching excited NCO was produced via both dissociation pathways.

Key words: Photodissociation dynamics, Rydberg tagging time-of-flight spectroscopy, Internal conversion

I. INTRODUCTION

Isocyanic acid (HNCO) plays an important role in combustion and atmospheric chemistry, such as, the applications in removal of NO_x compounds from combustion exhaust gases [1−3], and potentially harmful exposure of humans to HNCO in ambient air as a consequence of biomass burning, biofuel usage and tobacco usage [4]. In addition to the practical importance, photodissociation of HNCO is fundamentally interesting because of the variety of dissociation processes involving different electronic transitions. The electronic absorption spectrum of HNCO originates at about 280 nm, and this first absorption band extends to wavelengths shorter than 200 nm, which has been assigned to the transition from the ground electronic state to the first singlet excited state, $S_1(^1A'')$←$S_0(^1A')$ [5−7]. Photodissociation of HNCO in this spectral region may evolve on two or three of the potential energy surfaces (PESs) of S_0, S_1 and the first triplet excited state $T_1(3A'')$, and lead to three dissociation channels (the dissociation energies D_0 are from Ref.[8]),

$$\begin{aligned} \mathrm{HNCO}+h\nu &\rightarrow \mathrm{NH}(X^3\Sigma^-)+\mathrm{CO}(X^1\Sigma^+) \quad (1)\\ &\quad D_0=30060\pm25\ \mathrm{cm}^{-1}\\ &\rightarrow \mathrm{H}(^2\mathrm{S})+\mathrm{NCO}(X^2\Pi) \quad (2)\\ &\quad D_0=38370\pm25\ \mathrm{cm}^{-1}\\ &\rightarrow \mathrm{NH}(a^1\Delta)+\mathrm{CO}(X^1\Sigma^+) \quad (3)\\ &\quad D_0=42750\pm25\ \mathrm{cm}^{-1} \end{aligned}$$

during which internal conversion (IC) or intersystem crossing (ISC) can be involved [9, 10]. The energy level diagram for HNCO and its dissociation products is shown in FIG. 1.

Spin-forbidden channel (1) comes from dissociation on triplet state T_1 following electronic transitions including ISC, and is still the major channel in the energy region just above the opening of channel (2) [11, 12]. The pathway via IC from S_1 to S_0 then ISC from S_0 to T_1 was suggested by Kaledin *et al.* [9] in their theoretical research. For spin-allowed channels (2) and (3), S_1 state correlates with both of them [13]. There is a large barrier (>8140 cm^{-1}) exiting in the channel (2) dissociation pathway on S_1 PES, and a low barrier of about 470 cm^{-1} for channel (3) [8]. Thus, for excitation energy below the large barrier, channel (2) can only be accessed by dissociation on S_0 following IC from S_1 to S_0 [14], whereas for sufficiently high excitation energy, the direct dissociation on S_1 becomes possible [15, 16],

†These authors contributed equally to this work.
*Author to whom correspondence should be addressed. E-mail: kjyuan@dicp.ac.cn

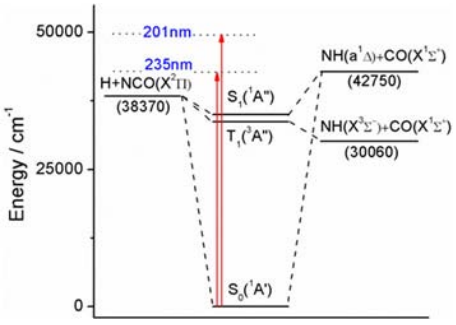

FIG. 1 Energy level diagram for the HNCO dissociation processes (adapted from Ref.[8]). The red arrow covers a range of wavelengths investigated in this photolysis study.

and competition between the two pathways is expected [17]. Similarly, the dissociation resulting in channel (3) initially takes place on S_0 [14], while above the small barrier, direct dissociation pathway on S_1 opens and dominates quickly [18−20].

In contrast to the extensive experimental and theoretical studies on the photodissociation dynamics of HNCO [8−27], for the DNCO system, considerably less dynamical information is available, and the analogue dissociation channels from S_1 state should be

$$\mathrm{DNCO} + h\nu \rightarrow \mathrm{ND}(X^3\Sigma^-) + \mathrm{CO}(X^1\Sigma^+) \quad (4)$$

$$\mathrm{D}(^2\mathrm{S}) + \mathrm{NCO}(X^2\Pi) \quad (5)$$

$$\mathrm{ND}(a^1\Delta) + \mathrm{CO}(X^1\Sigma^+) \quad (6)$$

Dixon and Kirby [5] attempted to photograph the absorption spectrum of DNCO from 265 nm to shorter wavelengths. Bohn and Stuhl [28] reported the vibrational population distribution of ND ($a^1\Delta$) radical from photodissociation of DNCO at 193 nm. Sanov *et al.* [29] examined the photodissociation of jet-cooled DNCO at 243.1 nm by photofragment ion imaging of D atom and suggested predissociation via S_0 state should be dominant. Brownsword *et al.* [30] investigated the photodissociation dynamics of DNCO at room temperature at 193 and 248 nm using the laser-induced fluorescence technique. The D atom product quantum yield, the fraction of the available energy released as product translational energy and the value of anisotropy parameter β for channel (5) were determined, and comparisons were made with the results of HNCO. The results were consistent with direct dissociation on S_1 surface after excitation at 193 nm and on the other hand decomposition from a predissociative state after excitation at 248 nm.

In the present work, we reinvestigated the photodissociation dynamics of DNCO over a broad range of wavelength, 200−235 nm, not yet available from the previous studies to the best of our knowledge, using high resolution D-atom Rydberg tagging time-of-flight technique, in order to shed light on the competitive mechanism changing for channel (5) and examine the effect of isotopic substitution on the photodissociation dynamics.

II. EXPERIMENTS

The photodissociation dynamics of D atom elimination channel from DNCO at photolysis wavelengths in the range of 200−235 nm were investigated using the D-atom Rydberg tagging time-of-flight (DRTOF) technique, which has been described in detail elsewhere [31−35]. Only a brief description is presented here. In this experiment, the DNCO molecular beam was formed by expanding ∼3% DNCO/Ar mixture at a stagnation pressure of ∼760 torr via a pulsed general valve. After passing through a skimmer, the pulsed DNCO molecular beam was intercepted by the photolysis laser beam, which was generated by frequency doubling (for photolysis wavelengths in the range of 219−235 nm) or tripling (for 200−211 nm) of an Nd:YAG laser pumped dye laser output. The nascent D atom products in the photolysis region were excited from the ground state to a high Rydberg state via a two-step excitation [36−38]. In the first excitation step, the D atoms were excited to the n=2 state by a 121.6 nm laser generated by the different four wave mixing (DFWM) method of 212.5 and 846 nm laser in a gas cell filled with Kr/Ar mixture with the mixing ratio of 1:3, in which two photons of 212.5 nm are in resonance with the Kr 4p-5p[1/2,0] transition. In the second step, the D (n=2) atoms were sequentially excited to a high Rydberg state with n≈50 by a ∼365 nm laser. The neutral Rydberg D atoms, following a field-free flying path of about 333 mm, were field ionized in front of a microchannel plate (MCP) detector. The signal received by the MCP was amplified by a fast preamplifier, and counted by a multichannel scaler. Since 212.5 nm and 121.6 nm light also generate D atom products from DNCO, the 212.5 nm laser was attenuated, thus the 121.6 nm light intensity was also decreased, and the background subtraction can be achieved easily by tuning the photolysis laser on and off.

DNCO was prepared by allowing a saturated aqueous solution of KNCO (freshly prepared using D_2O) to drop slowly into concentrated deuterated phosphoric acid (D_3PO_4) at room temperature [40−42]. The gaseous products were collected in a liquid nitrogen trap at −196 °C. Impurities were removed by trap-to-trap distillations from −60 °C to −120 °C. The resulting DNCO sample was stored in a stainless steel cylinder cooled to liquid nitrogen temperature to prevent polymerization. During the experiments, the molecular beam was generated by bubbling pure Ar gas through the sample kept in a container cooled by a −50 °C low-temperature bath. The purity was checked by mass spectrometry (SRS, RGA200).

III. RESULTS

A. Product translational energy distribution

TOF spectra of the D atom products from photodissociation of DNCO at different photolysis wave-

DOI:10.1063/1674-0068/cjcp1904074

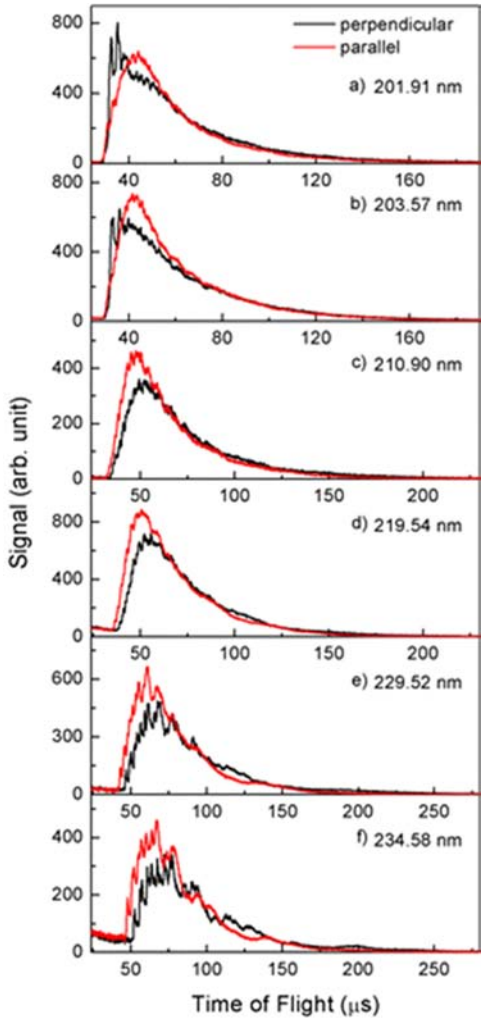

FIG. 2 Time-of-flight spectra of D atom products from photodissociation of DNCO at (a) 201.91 nm, (b) 203.57 nm, (c) 210.90 nm, (d) 219.54 nm, (e) 229.52 nm, and (f) 234.58 nm with the detection direction perpendicular (black line) and parallel (red line) to the photolysis laser polarization.

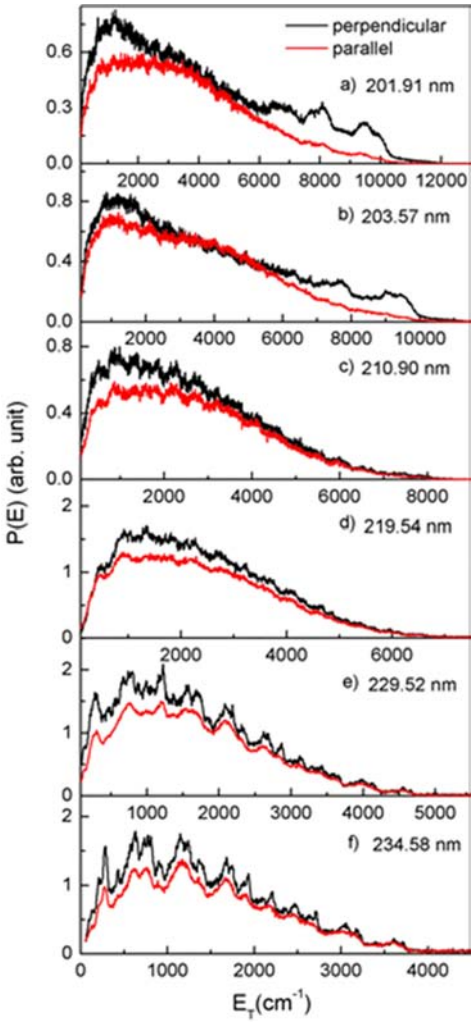

FIG. 3 Total translational energy distributions for DNCO photodissociation with the detection direction perpendicular (black line) and parallel (red line) to the photolysis laser polarization at (a) 201.91 nm, (b) 203.57 nm, (c) 210.90 nm, (d) 219.54 nm, (e) 229.52 nm, and (f) 234.58 nm.

lengths between 200 and 235 nm were measured using the above experimental methods. FIG. 2 shows the D atom TOF spectra at both detection directions perpendicular and parallel to the photolysis laser polarization at 201.91, 203.57, 210.90, 219.54, 229.52 and 234.58 nm. For the photolysis wavelengths in the range of 210.90−234.58 nm, the TOF spectra show a partially resolved progression of peaks with weak anisotropy, which becomes more diffuse as the photon energy increases. At 203.57 and 201.91 nm, additional structures with significant anisotropy arise at early arriving time, suggesting the existence of another competitive photodissociation pathway.

The TOF spectra at all six photolysis wavelengths were converted to the total translational energy distributions, as shown in FIG. 3, using a computer program that includes allowance for the velocity of the molecular beam. Assuming that the starting point of the total translational energy distribution at the high energy side corresponds to the rovibrational ground state of NCO($X^2\Pi$) product and thus equals to the available energy for photodissociation of DNCO at the corresponding wavelength, the dissociation energy D_0(D-NCO) can be therefore determined to be (38853±30) cm^{-1}. The difference between this value and that of D_0(H-NCO) is consistent with the difference of ∼500 cm^{-1} in the zero-point energy of the two systems [44].

There are two distinguishable features in FIG. 3: a nearly statistical distribution peaking at low translational energy shown at all photolysis wavelengths involved in this work, and an additional structured distribution at high translational energy only present at the high excitation energies. The former is similar to

DOI:10.1063/1674-0068/cjcp1904074

that observed in photodissociation of HNCO [8, 17] and should be attributed to dissociation on S_0 state following IC from S_1 to S_0 state. Considering the resemblance between DNCO and HNCO, the latter may come from direct dissociation on S_1 state, which occurs only when the excitation energy is high enough to overcome the large barrier in the D+NCO dissociation pathway on the S_1 PES [15, 17]. According to FIG. 3 (b) and (c), the barrier height was estimated to be in the range of 8548−10254 cm^{-1}. From the translational energy distributions, the fraction of the available energy released into the translational energy, f_T, can be determined to be about 0.37, 0.35, 0.30, 0.34, 0.35, and 0.37 for the photolysis wavelengths of 201.91, 203.57, 210.90, 219.54, 229.52, and 234.58 nm, respectively.

B. Product anisotropy distribution

In a one-photon molecular photodissociation process, the photodissociation product detected at an angle in the center-of-mass frame (θ_{cm}) relative to the photolysis laser polarization can be represented by the following formula:

$$\psi(E_T, \theta_{cm}) = \sigma(E_T)[1 + \beta(E_T)P_2(\cos\theta_{cm})] \qquad (7)$$

where $\sigma(E_T)$ is the product translational energy distribution, $\beta(E_T)$ is the translational energy dependent anisotropy parameter, and $P_2(\cos\theta_{cm})=(3\cos^2\theta_{cm}-1)/2$ is the second order Legendre polynomial. The value of β is between -1 and 2. $\beta=-1$ corresponds to a pure perpendicular transition while $\beta=2$ corresponds to a pure parallel transition. In this experiment, the translational energy distributions with the detection axis perpendicular and parallel to the photolysis laser polarization were measured, therefore, $\beta(E_T)$ can be calculated.

FIG. 4 shows the anisotropy parameter as a function of the total translational energy, $\beta(E_T)$, for the six photolysis wavelengths. At 210.90−234.58 nm, nearly isotropic angular distributions were observed with $\beta\approx-0.1$, suggesting a relatively slow dissociation process, in accordance with the predissociation pathway involving IC from S_1 to S_0. At 203.57 and 201.91 nm, the anisotropy parameter shows near zero value at lower translational energy and large negative value ($\beta\approx-0.75$) at higher translational energy, indicating two dissociation mechanisms are involved in this wavelength region, *i.e.*, predissociation via IC from S_1 to S_0 state followed by dissociation on S_0 surface, and direct dissociation on S_1 surface.

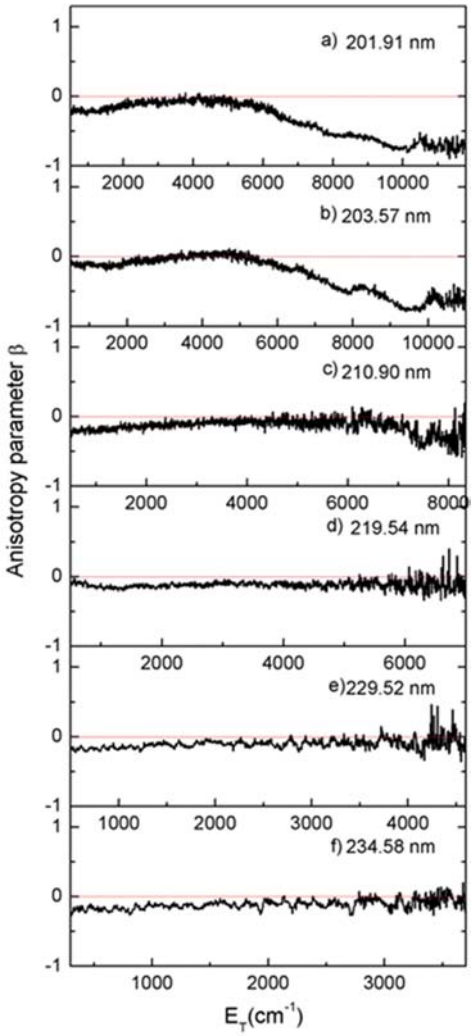

FIG. 4 Anisotropy parameter β as a function of the total translational energy from the photodissociation of DNCO at (a) 201.91 nm, (b) 203.57 nm, (c) 210.90 nm, (d) 219.54 nm, (e) 229.52 nm, and (f) 234.58 nm.

IV. DISCUSSIONS

According to the energy conservation, the internal energy distribution of the NCO product can be determined from the total translational energy distribution. FIG. 5 shows the NCO internal energy distribution from the photodissociation of DNCO at 234.58 nm. As previously mentioned, this excitation energy is insufficient to overcome the barrier along the D+NCO dissociation pathway on S_1 surface, and predissociation via IC from S_1 to S_0 should dominate. The first two peaks at the low internal energy in FIG. 5 are separated by ∼95 cm^{-1}, coincident with the spin-orbit split between $^2\Pi_{3/2}$ and $^2\Pi_{1/2}$ states of NCO(0, 0, 0) (here (ν_1, ν_2, ν_3) corresponds to the quantum number of symmetric stretching, bending and asymmetric stretching of NCO products, respectively). Most of the peaks in FIG. 5 can be assigned to the fine structures of vibrational levels of progressions of bending mode ν_2 with zero or one quanta of stretching mode ν_1 or ν_3, according to the spectroscopic values reported in the laser fluorescence excitation spectra research [45]. The tentative assignments are shown in FIG. 5.

Previous theoretical investigations showed that the potential minimum on S_1 surface corresponds to con-

DOI:10.1063/1674-0068/cjcp1904074

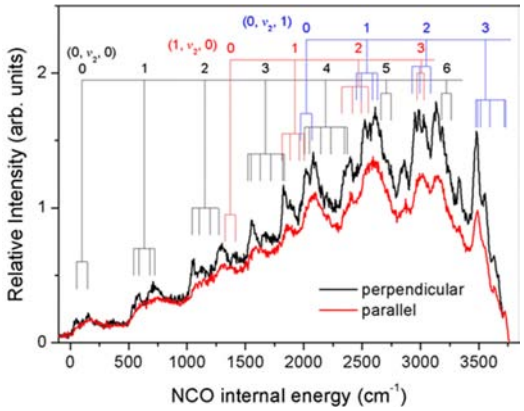

FIG. 5 NCO internal energy distributions for the photodissociation of DNCO at 234.58 nm with the detection direction perpendicular (black line) and parallel (red line) to the photolysis laser polarization. The vibrational levels (ν_1, ν_2, ν_3) of NCO($X^2\Pi$) split into different components by the combination of spin-orbit and Renner-Teller interactions. (ν_1: symmetric stretching, ν_2: bending, and ν_3: asymmetric stretching).

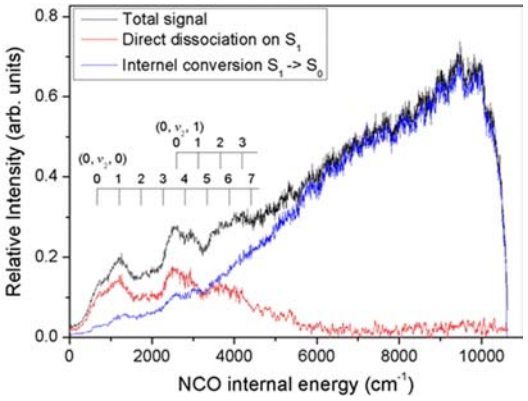

FIG. 6 NCO internal energy distributions for the photodissociation of DNCO at 201.91 nm (θ_{cm}=54.7°). Two competitive dissociation pathways contribute to the total signal (black line): direct dissociation on S_1 surface (red line) and internal conversion from S_1 to S_0 state followed by dissociation on S_0 surface (blue line). The observed structures can be assigned to the NCO vibrational levels.

figurations with bent N−C−O (125.1° for *trans*- and 129.8° for *cis*-HNCO), quite different from the ground state geometry with almost linear N−C−O [21]. In addition, the N−C and C−O equilibrium bond lengths are slightly larger on the S_1 state compared with that on the ground state [22]. Similar configurations should exist in the case of DNCO, which are confirmed by the experimental observation that the NCO product is mainly bending and a little stretching excited.

The NCO internal energy distribution from the photodissociation of DNCO at 201.91 nm can also be obtained from the total translational energy distribution and is shown in FIG. 6. Two components are observed: the lower internal energy distribution with several partially resolved peaks corresponding to the direct dissociation on S_1 surface and the higher internal energy distribution peaking at ∼9500 cm^{-1} ascribed to the predissociation pathway via S_1→S_0 IC followed by decomposition on S_0 surface, based on the analysis in the previous sections. Remarkably different anisotropy parameters for these two dissociation pathways make deconvolution of the NCO internal energy distribution possible (FIG. 6). Obviously, predissociation pathway is still dominant, while the direct dissociation pathway only makes a minor contribution, responsible for ∼18% of the total products.

The partially resolved peaks at relatively low internal energy in FIG. 6 can be assigned to the vibrational levels of the ground electronic state NCO(X), but the fine structures cannot be resolved in this spectrum. Possible assignments are also shown in FIG. 6, employing the vibrational frequencies of ν_1 (534 cm^{-1}), ν_2 (1270 cm^{-1}) and ν_3 (1922 cm^{-1}) obtained from the laser-induced fluorescence experiments.

Comparing the photodissociation of DNCO in this work and that of HNCO in the same photolysis wavelength region reported previously [17], similar dynamics is observed. However, significant differences are also present. The direct dissociation pathway on S_1 surface can be clearly observed at 210.02 nm for the photodissociation of HNCO, but for DNCO, this pathway is not open yet at 210.90 nm, indicating that higher excitation energy is needed for opening the direct dissociation pathway in the case of DNCO. Besides, the fraction of products from the direct dissociation pathway at ∼202 nm for DNCO is significantly smaller (∼18%) than that for HNCO (∼36%) [17], indicating the nonadiabatic couplings between S_1 and S_0 PESs are affected by isotope effect. In addition, the fraction of the available energy deposited into the total translational energy for DNCO is 0.37 at around 202 nm, also smaller than that for HNCO at the same wavelength (f_T=0.47 [17]). This is probably because the different masses of H and D atoms. The D atom dissociating its partner NCO will tend to have a higher internal energy than that from HNCO.

V. CONCLUSION

In this work, the photodissociation dynamics of DNCO at 200−235 nm have been investigated using the D-atom Rydberg tagging time-of-flight technique. The total translational energy distributions and the product angular anisotropy parameters have been determined by measuring the TOF spectra of the D atom products at both detection directions perpendicular and parallel to the photolysis laser polarization. Generally, the results are similar to the previously reported experimental results of HNCO. The predissociation pathway via internal conversion from S_1 to S_0 state followed by decomposition on S_0 surface is involved in the whole range of

DOI:10.1063/1674-0068/cjcp1904074

photolysis wavelength in the present work, while the direct dissociation pathway on S_1 surface can be observed only at sufficiently high excitation energy. The partially resolved structures in the NCO internal energy distributions can be assigned to bending with a little stretching excitation of the NCO product. The higher threshold of the direct dissociation pathway for the photodissociation of DNCO than that of HNCO is observed. The observations in this work have provided valuable information on the isotope affected nonadiabatic dynamics.

VI. ACKNOWLEDGMENTS

This work was supported by the Strategic Priority Research Program of the Chinese Academy of Sciences (No.XDB17000000), the Chemical Dynamics Research Center (No.21688102), the National Natural Science Foundation of China (No.21873099 and NO.21673232), and the Youth Innovation Promotion Association (No.2014160).

[1] B. S. Haynes, Combust. Flame **28**, 113 (1977).
[2] R. A. Perry and D. L. Siebers, Nature **324**, 657 (1986).
[3] J. A. Miller and C. T. Bowman, Int. J. Chem. Kinet. **23**, 289 (1991).
[4] J. M. Roberts, P. R. Veres, A. K. Cochran, C. Warneke, I. R. Burling, R. J. Yokelson, B. Lerner, J. B. Gilman, W. C. Kuster, R. Fall, and J. de Gouw, Pro. Nat. Acad. Sci. USA **108**, 8966 (2011).
[5] R. N. Dixon and G. H. Kirby, Trans. Faraday Soc. **64**, 2002 (1968).
[6] J. W. Rabalais, J. R. McDonald, and S. P. McGlynn, J. Chem. Phys. **51**, 5103 (1969).
[7] S. P. McGlynn, J. W. Rabalais, J. R. McDonald, and V. M. Scherr, Chem. Rev. **71**, 73 (1971).
[8] M. Zyrianov, T. Droz-Georget, and H. Reisler, J. Chem. Phys. **110**, 2059 (1999).
[9] A. L. Kaledin, Q. Cui, M. C. Heaven, and K. Morokuma, J. Chem. Phys. **111**, 5004 (1999).
[10] M. Zyrianov, T. Droz-Georget, and H. Reisler, J. Chem. Phys. **106**, 7454 (1997).
[11] M. Zyrianov, A. Sanov, T. Droz-Georget, and H. Reisler, J. Chem. Phys. **110**, 10774 (1999).
[12] R. A. Brownsword, T. Laurent, R. K. Vatsa, H. R. Volpp, and J. Wolfrum, Chem. Phys. Lett. **258**, 164 (1996).
[13] J. J. Klossika and R. Schinke, J. Chem. Phys. **111**, 5882 (1999).
[14] M. Zyrianov, T. Droz-Georget, A. Sanov, and H. Reisler, J. Chem. Phys. **105**, 8111 (1996).
[15] J. Zhang, M. Dulligan, and C. Wittig, J. Phys. Chem. **99**, 7446 (1995).
[16] R. A. Brownsword, T. Laurent, R. K. Vatsa, H. R. Volpp, and J. Wolfrum, Chem. Phys. Lett. **249**, 162 (1996).
[17] S. Yu, S. Su, Y. Dorenkamp, A. M. Wodtke, D. Dai, K. Yuan, and X. Yang, J. Phys. Chem. A **117**, 11673 (2013).
[18] D. Conroy, V. Aristov, L. Feng, A. Sanov, and H. Reisler, Acc. Chem. Res. **34**, 625 (2001).
[19] T. A. Spiglanin, R. A. Perry, and D. W. Chandler, J. Phys. Chem. **90**, 6184 (1986).
[20] S. S. Brown, H. L. Berghout, and F. F. Crim, J. Chem. Phys. **105**, 8103 (1996).
[21] J. J. Klossika, H. Flöthmann, C. Beck, R. Schinke, and K. Yamashita, Chem. Phys. Lett. **276**, 325 (1997).
[22] J. E. Stevens, Q. Cui, and K. Morokuma, J. Chem. Phys. **108**, 1452 (1998).
[23] T. Droz-Georget, M. Zyrianov, H. Reisler, and D. W. Chandler, Chem. Phys. Lett. **276**, 316 (1997).
[24] T. H. Droz-Georget, M. Zyrianov, A. Sanov, and H. Reisler, Berichte der Bunsengesellschaft für physikalische Chemie **101**, 469 (1997).
[25] W. S. Drozdoski, A. P. Baronavski, and J. R. McDonald, Chem. Phys. Lett. **64**, 421 (1979).
[26] G. T. Fujimoto, M. E. Umstead, and M. C. Lin, Chem. Phys. **65**, 197 (1982).
[27] Z. Zhang, Z. Chen, C. Huang, Y. Chen, D. Dai, D. H. Parker, and X. Yang, J. Phys. Chem. A **118**, 2413 (2014).
[28] B. Bohn and F. Stuhl, J. Phys. Chem. **97**, 4891 (1993).
[29] A. Sanov, T. Droz-Georget, M. Zyrianov, and H. Reisler, J. Chem. Phys. **106**, 7013 (1997).
[30] R. A. Brownsword, M. Hillenkamp, T. Laurent, R. K. Vatsa, and H. R. Volpp, J. Chem. Phys. **106**, 4436 (1997).
[31] L. Schnieder, K. Seekamp-Rahn, E. Wrede, and K. H. Welge, J. Chem. Phys. **107**, 6175 (1997).
[32] K. Yuan, R. N. Dixon, and X. Yang, Acc. Chem. Res. **44**, 369 (2011).
[33] K. Yuan, Y. Cheng, L. Cheng, Q. Guo, D. Dai, X. Wang, X. Yang, and R. N. Dixon, Proc. Natl. Acad. Sci. USA **105**, 19148 (2008).
[34] H. Wang, Y. Yu, Y. Chang, S. Su, S. Yu, Q. Li, K. Tao, H. Ding, J. Yang, G. Wang, L. Che, Z. He, Z. Chen, X. Wang, W. Zhang, D. Dai, G. Wu, K. Yuan, and X. Yang, J. Chem. Phys. **148**, 124301 (2018).
[35] K. Yuan, L. Cheng, Y. Cheng, Q. Guo, D. Dai, and X. Yang, J. Chem. Phys. **131**, 074301 (2009).
[36] Y. Chang, Y. Yu, H. Wang, X. Hu, Q. Li, J. Yang, S. Su, Z. G. He, Z. C. Chen, L. Che, X. Wang, W. Zhang, G. Wu, D. Xie, M. N. R. Ashfold, K. Yuan, and X. Yang, Nat. Commun. **10**, 1025 (2019).
[37] M. N. R. Ashfold, K. Yuan, and X. Yang, J. Chem. Phys. **149**, 080901 (2018).
[38] H. Wang, S. Su, S. Yu, L. Che, G. Wu, K. Yuan, X. Yang, and T. K. Minton, Chin. J. Chem. Phys. **32**, 151 (2019).
[39] J. P. Marangos, N. Shen, H. Ma, M. H. R. Hutchinson, and J. P. Connerade, J. Opt. Soc. Am. B **7**, 1254 (1990).
[40] R. A. Ashby and R. L. Werner, J. Mol. Spec. **18**, 184 (1965).
[41] B. Krakow, R. C. Lord, and G. O. Neely, J. Mol. Spec. **27**, 148 (1968).
[42] W. D. Woolley and R. A. Back, Can. J. Chem. **46**, 295 (1968).
[43] S. A. Harich, D. W. H. Hwang, X. Yang, J. J. Lin, X. Yang, and R. N. Dixon, J. Chem. Phys. **113**, 10073 (2000).
[44] A. L. L. East, C. S. Johnson, and W. D. Allen, J. Chem. Phys. **98**, 1299 (1993).
[45] D. Patel-Misra, D. G. Sauder, and P. J. Dagdigian, J. Chem. Phys. **93**, 5448 (1990).
[46] R. A. Copeland and D. R. Crosley, Can. J. Phys. **62**, 1488 (1984).

DOI:10.1063/1674-0068/cjcp1904074